EUROfusion

EUROFUSION CP(15)04/01

A. Calvo et al.

Manufacturing of Self-Passivating Tungsten Based Alloys by Different Powder Metallurgical Routes

(18th May 2015 – 22nd May 2015)
Aix-en-Provence, France

This work has been carried out within the framework of the EUROfusion Consortium and has received funding from the Euratom research and training programme 2014-2018 under grant agreement No 633053. The views and opinions expressed herein do not necessarily reflect those of the European Commission.

Manufacturing of self-passivating tungsten based alloys by different powder metallurgical routes

A Calvo[1], N Ordás[1], I Iturriza[1], J Y Pastor[2], E Tejado[2], T Palacios[2] and C García-Rosales[1,*]

[1]*CEIT and TECNUN (University of Navarra), E-20018 San Sebastián, Spain*
[2]*Polytechnic University of Madrid and CIEMAT, E-28040 Madrid, Spain*

Abstract

Self-passivating tungsten based alloys will provide a major safety advantage compared to pure tungsten when used as first wall armour of future fusion reactors, due to the formation of a protective oxide layer which prevents the formation of volatile and radioactive WO_3 in case of a loss of coolant accident with simultaneous air ingress.

Bulk WCr10Ti2 alloys were manufactured by two different powder metallurgical routes: 1) mechanical alloying (MA) followed by HIP of metallic capsules, and 2) MA, compaction, pressureless sintering in H_2 and subsequent HIPing without encapsulation. Both routes resulted in fully dense materials with homogeneous microstructure and grain sizes of 300 nm and 1 µm, respectively. The content of impurities remained unchanged after HIP, but it increased after sintering due to binder residue. It was not possible to produce large samples by the second route due to difficulties in the uniaxial compaction stage. Flexural strength and fracture toughness measured on samples produced by the first route revealed a suctile-to-brittle-transition temperature (DBTT) of about 900°C. The strength increased from room temperature to 800°C, decreasing significantly in the plastic region. An increase of fracture toughness is observed around the DBTT.

PACS numbers: 81.05.Je, 52.40.Hf

* Corresponding author
Carmen García-Rosales
CEIT and Tecnun (University of Navarra)
Pº de Manuel Lardizabal, 15
200009 San Sebastian, Spain.
Tel.: +(34) 43 21 28 00
E-mail address: cgrosales@ceit.es

1. Introduction

Tungsten is the main candidate plasma facing material for the first wall (FW) armour of future fusion reactors such as DEMO [1]. However, the use of pure W involves a potential safety risk in case of a loss-of-coolant accident, after which several days because of the decay heat [2]. In such a situation, additional air ingress into the reactor vessel would lead to full armour oxidation and to therelease of highly activated and volatile tungsten oxides [3]. The use of self-passivating tungsten alloys can be a feasible alternative to avoid this important safety issue. In these alloys the additives would form a stable oxide scale at high temperatures upon accidental air ingress, protecting the underlying W alloy from fast oxidation and sublimation of WO_3.

In previous work [4]-[5] different bulk tungsten alloys of the systems W-Cr-Si and W-Cr-Ti were manufactured by mechanical alloying (MA) and densification by Hot Isostatic Pressing (HIP) after glass encapsulation. The addition of Cr and Si or Ti as alloying elements resulted in a reduction of the oxidation rate by several orders of magnitude at temperatures up to 1000°C compared to pure tungsten [4], [6]-[8], due to the growth of a protective oxide layer. However, glass encapsulation is not a suitable process to manufacture large samples due to their large weight, increasing the probability to leave out the capsule during HIPing. Thus, in the present work two different powder metallurgical (PM) routes are proposed as scalable methods to produce self-passivating tungsten alloys. The first route consists of MA followed by HIP of metallic capsules filled with the alloyed powder, whereas the second one consist of MA, compaction, pressureless sintering in H_2 and subsequent HIPing without encapsulation. In this case, the goal is to produce a material whose relative density is at least 92% after sintering and finally to obtain fully dense samples by HIP. A similar route is used in industrial processes, where tungsten powder is sintered at high temperatures for long times to achieve relative densities of at least 88%; the residual porosity is eliminated by subsequent working , which also contribute to increase ductility and reduce the ductile-to-brittle transition temperature (DBTT) [9]. Si tends to form brittle intermetallics with detrimental effect on the workability. For this reason, future efforts were concentrated on Si-free alloys

[8],[5]. In this work, W-Cr-Ti alloys of composition WCr10Ti2 (in wt.%) are manufactured by MA and densified through the two mentioned routes. A different composition with respect to previous work is employed to study the effect of Cr concentration on the self-passivating layer formation. In this paper, microstructure and impurity content of samples obtained by the two routes are compared, and thermal and mechanical properties of samples manufactured by the first route are shown.

2. Experimental details

Elemental powders of pure W (99.97%, 4.45 μm), Cr (99.95%, 74 μm) and Ti (99.5%, 40 μm) were used to produce samples of composition WCr10Ti2 (in wt.%). The starting powders were blended in a turbula mixer and mechanically alloyed under Ar atmosphere in a planetary ball mill Retsch PM400 using grinding jars and balls of WC. The MA parameters were those found as optimum for W-Cr-Ti systems in previous works [4],[5]. Samples of different geometries were produced with the milled powders by the two mentioned routes. For the first route (MA, can encapsulation and HIP), metal canisters of Ø 15 mm and 40 mm height filled with the alloyed powder were degassed at high vacuum, sealed and HIPed at 1300ºC for 1 h at 150 MPa. In the second one (MA, sintering in H_2 and HIP without encapsulation), the alloyed powder was uniaxially compacted at various pressures to cylinders of ∅16 and 20 mm and ~4 mm height, degassed at high vacuum and sintered at 1600ºC for 2 h in H_2 atmosphere. Different organic binders were used for compaction. After sintering, the samples were HIPed without encapsulation at 1300ºC for 1 h at 150 MPa.

The particle size distribution of the milled powders was measured by laser difraction. The oxygen and nitrogen contents of the mechanically alloyed powders and bulk materials obtained by both routes were determined using the inert gas fusion method (ASTM E1569, measured with a LECO TC-400), and the carbon content by the combustion method (ASTM E1019, measured with a LECO CS-200). Powders and bulk samples were characterized by field emission gun SEM (FEG-SEM), energy dispersive X-ray spectroscopy (EDX) and X-ray diffraction (XRD). The open porosity after sintering was measured by He pycnometry, and the relative density of all samples was determined from the

geometrical and theoretical densities. The grain size of the different phases present in the materials was determined by quantitative metallography.

Vickers microhardness measurements on polished surfaces of HIPped material were performed applying a load of 0.5 kg for 5 s. The elastic modulus was measured up to 1000°C by the Impulse Excitation Technique (IET) on samples of dimensions $5 \times 2 \times 30$ mm^3. Three-point bending (TPB) tests were performed on smooth and single edge laser-notched beams [10] (nominal dimensions $2.5 \times 2.5 \times 30$ mm^3) over the temperature range 20°C to 1100°C under high vacuum (inert atmosphere). All tests were performed in displacement control at a fixed loading rate of 100 μm/min with 25 mm span width. Flexural strength was computed by Euler-Bernoulli equations for slender beams up to failure. However, when yield stress was exceeded, 0.2% strength offset was reported. To calculate the appropriate fracture toughness (K_{IC}), the maximum load and the initial notch length for each test, measured previously via FEG-SEM, were computed in the formula proposed by Guinea et al. [11]. Finally, the fracture surfaces of all tested specimens were extensively examined by FEG-SEM.

3. Results and discussion

Mechanically alloyed powders of composition WCr10Ti2 in wt% (WCr27Ti6 in at.%) were used to produce dense materials by the two PM routes. The average particle size of the powders after MA is 6.4 μm. Their O, C and N contents are shown in Table 1.

Table 1. Relative density, microhardness and oxygen, nitrogen and carbon contents of WCr10Ti2 samples produced by the two PM routes at different processing steps

	Relative Density (%)	Microhardness ($HV_{0.5}$)	Impurities (wt.%)		
			O	N	C
MA	-	-	0.11 ± 0.01	0.011 ± 0.001	0.016 ± 0.003
HIP	100	1015 ± 5	0.11 ± 0.01	0.010 ± 0.001	0.017 ± 0.002
P.Sintering	93	-	0.25 ± 0.06	0.012 ± 0.002	0.06 ± 0.01
P.Sinter.+HIP	100	865 ± 5	0.25 ± 0.05	0.011 ± 0.001	0.06 ± 0.01

3.1. MA + HIP with can encapsulation

The mechanically alloyed powders were can encapsulated and HIPed at 1300ºC for 1 h achieving relative densities above 99%, i.e. the samples can be

considered fully dense within the experimental error. The O, C and N contents of the as-HIPed material (Table 1) indicate that there is no uptake of contaminants during encapsulation and HIPing. The amounts of O and C after HIP are comparable to those reported in previous works using glass (instead of can) encapsulation [4],[5].

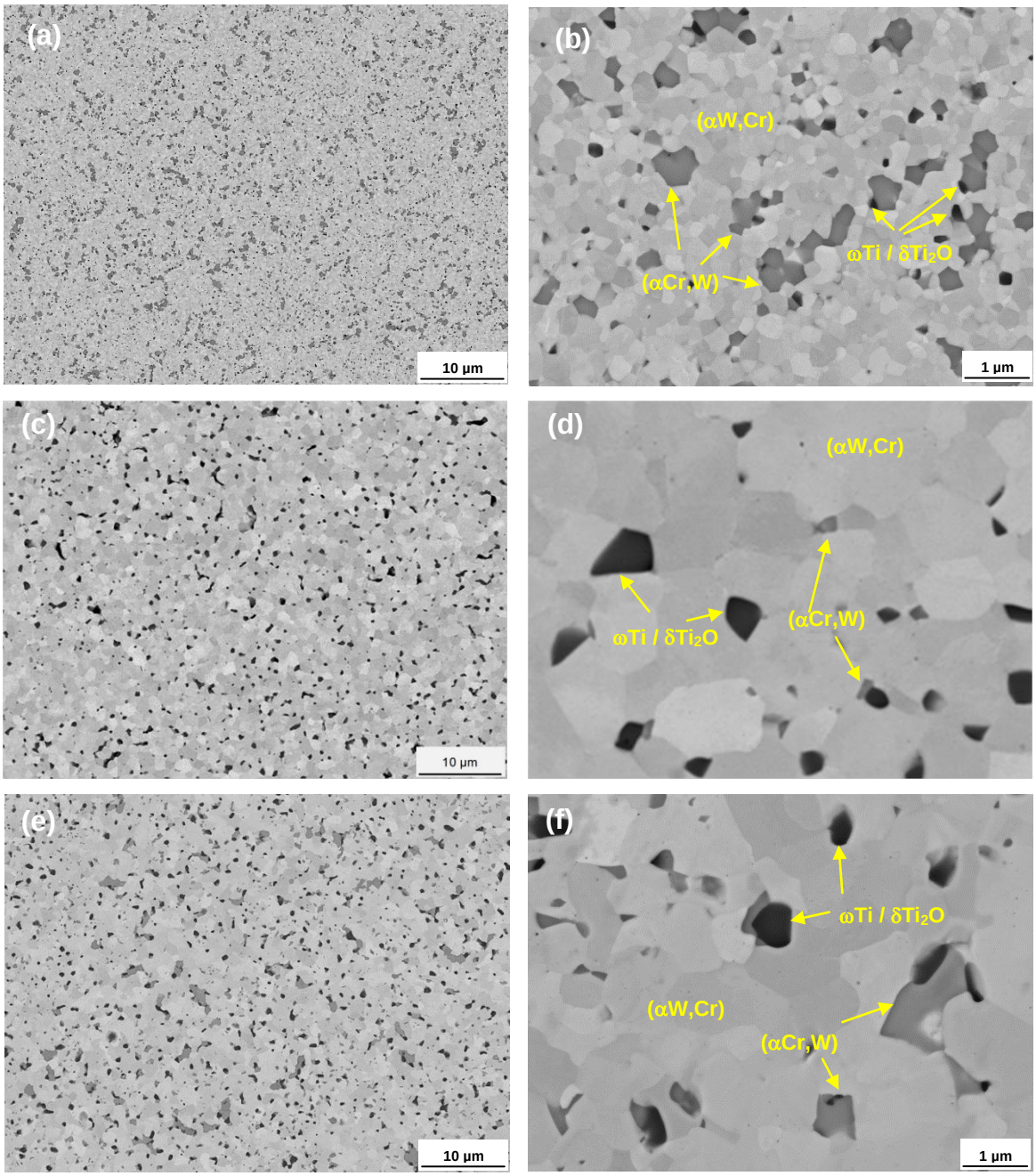

Figure 1. BSE-SEM images of WCr10Ti2 alloy after HIP at 1300ºC (a-b), after sintering at 1600ºC (c-d) and after sintering at 1600ºC + HIP at 1300ºC (e-f)

The microstructure of WCr10Ti2 samples is shown in Fig. 1 (a,b). A very fine and homogenous microstructure with grain size below 300 nm can be appreciated. As already found in previous work for a slightly different composition [5], the material is composed of three phases, identified by EDX as a W-rich phase with Cr in solution (bright grey majority phase in Fig. 1 (a,b)), a Cr-rich phase with W in solution (dark grey discontinuous phase) and a minority Ti-rich phase (black), which is mainly found in connection with the Cr-rich phase. EDX analysis of this Ti-rich phase evidences the presence of oxygen.

In Fig. 2 the XRD spectra of the initial powders, the powders after MA and the bulk materials produced with the two routes are compared. After MA a single bcc phase is observed with broad peaks shifted to higher 2θ values compared to the pure W phase indicating the dissolution of Cr in the W lattice; Ti is most probably also dissolved in W, but the 2θ shift produced by the small amount of Ti present in the mix would not be appreciated due to the similar lattice parameters of W and the high temperature bcc Ti phase [12]. The amount of Cr dissolved in the W lattice can be estimated from the shift of the XRD peaks using the Vegard's law [13], and is about 20 at.%, i.e. after MA a supersaturated (αW,Cr) phase is formed. The missing Cr amount of about 9 at.% is probably found in the initial pure Cr phase, which may have also W in solution and whose peaks cannot be appreciated due to the broadening induced by the MA process.

After HIPing at 1300°C the broad (αW,Cr) peak present after MA is shifted to lower 2θ values indicating a decrease in the Cr content, which is now of the order of 15 at.%, and a (αCr,W) phase containing about 22 at.% W dissolved in bcc Cr emerges. The peaks after HIP are still quite broad suggesting that a homogeneous phase composition has not yet been achieved. Nevertheless, the compositions of the (αW,Cr) and (αCr,W) phases are close to those expected at equilibrium at 1300°C as determined with the Thermo-Calc software [14] using the SSOL4 solutions database. The identification of the Ti-rich phase by XRD is not evident since only one not overlapping peak is obvious at $2\theta \approx 36°$. In previous work [5] this phase has been identified as ω-Ti, a metastable phase formed both in the Ti-W and Ti-Cr system during quenching from the bcc high temperature phase [15]. Nevertheless, the equiaxed form and size of the Ti-rich

grains indicate that this phase nucleates at high temperature at the same time as the (αW,Cr) and (αCr,W) phases. The ω-Ti phase is also a high-pressure phase formed from the parent bcc Ti phase [15]. According to EDX the whole oxygen content of the alloy seems to be associated to this phase. From all possible Ti-oxides, δ-Ti_2O [16] is the one better matching the XRD peaks. In this oxide the Ti subarray is identical to the high-pressure ω-Ti phase [17], and according to [18] the oxygen provides the pressure medium that stabilizes this phase. Taking into account the Ti and O contents in the alloy of 2 and 0.11 wt.% respectively (6 and 1 at.% respectively), it becomes clear that only 2 at.% Ti can form δ-Ti_2O and the remaining 4 at.% are possibly in form of ω-Ti or in solution with W and Cr as expected from the phase diagrams.

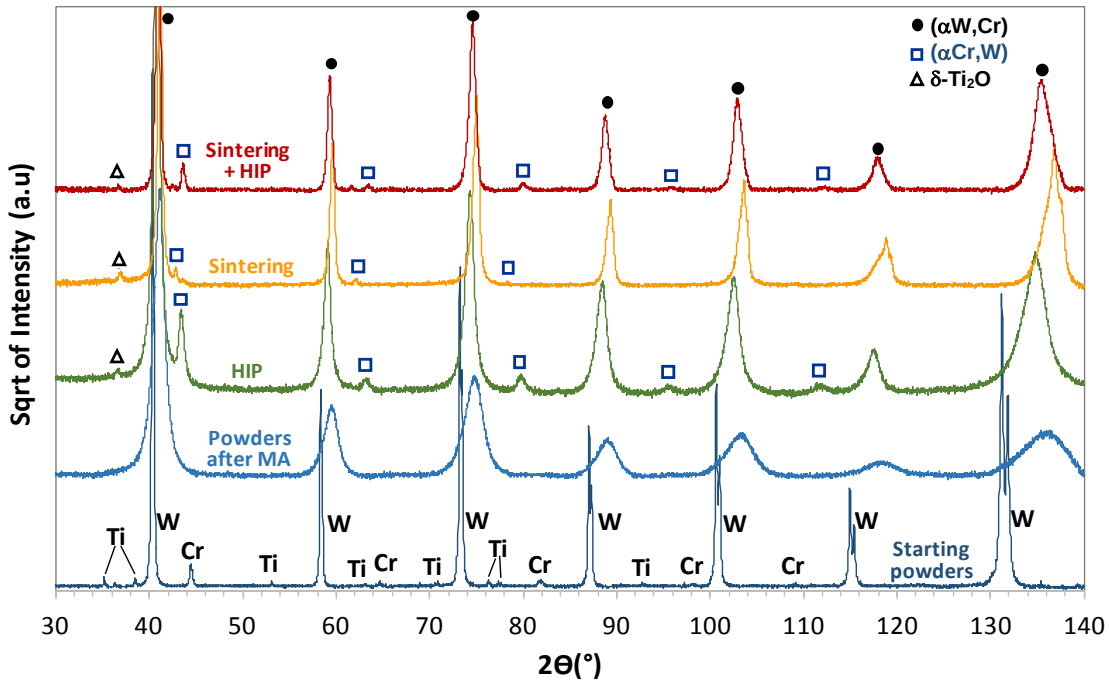

Figure 2. XRD spectra of WCr10Ti2 samples after HIP at 1300ºC, sintering at 1600ºC and sintering at 1600ºC + HIP at 1300ºC

The Vickers microhardness of HIPed WCr10Ti2 samples was measured at room temperature (Table 1). The microhardness is significantly higher than the one of pure recrystallized tungsten (~380 kg/mm^2 (HV30)) [9]. However, the hardness of polycrystalline tungsten increases appreciably with decreasing grain size following a Hall-Petch relationship

$$H = H_0 + K_H l^{-\frac{1}{2}} \quad (1)$$

with $H_0 =$ 350 kg/mm^2, $K_H =$ 10 kg·mm$^{-3/2}$ and l being the average grain diameter [9]. Taking into account the submicron grain size of the WCr10Ti2 alloy (average grain size 209 nm), the measured hardness is well in line with that of pure tungsten for the same grain size.

Samples of the WCr10Ti2 alloy produced by the first PM route were manufactured to explore its mechanical response by non-standard three-point bending tests as well as to measure the elastic modulus by IET. It should be noted that, while normally the MA process results in homogeneous powders with low amounts of heterogeneities (giving rise to microstructures like in Fig. 1a), the powder batch produced for these samples exhibited abnormally large amounts of heterogeneities, which were detected once the samples were cut out of the HIPed cylinder. These heterogeneities may act as crack initiation defects and so the resulting strength values will most probably be underestimated.

In Fig. 3 the elastic modulus as a function of temperature is shown. The form of the curve is very similar to that of polycrystalline tungsten [9] while the values of the WCr10Ti2 alloy are 19-20% lower in the measured temperature range.

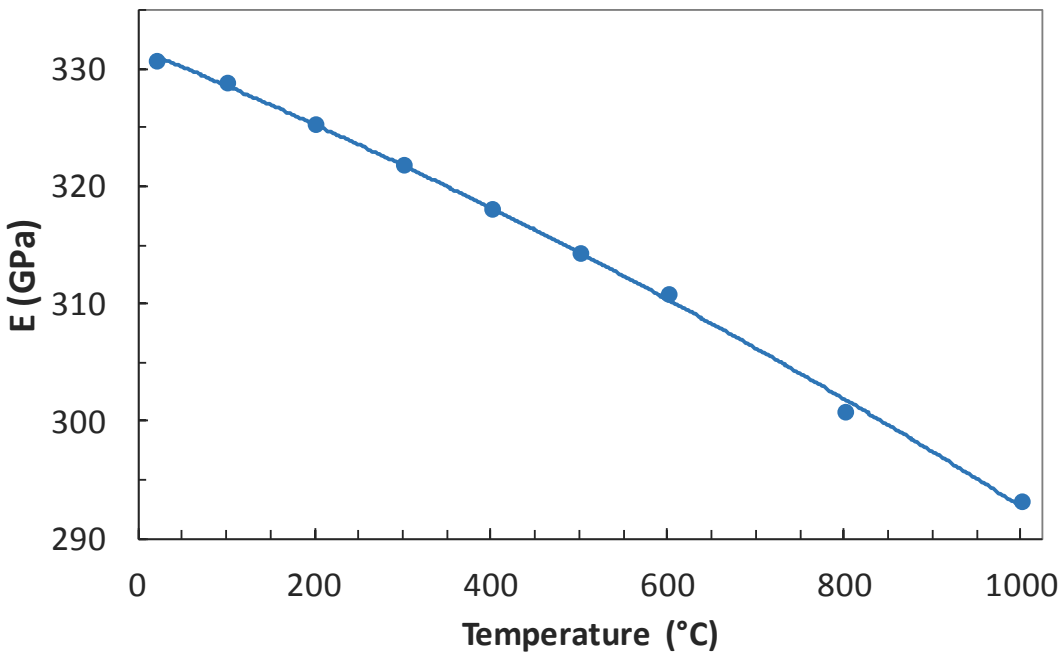

Figure 3. Elastic modulus of WCr10Ti2 after HIP at 1300°C as a function of temperature.

The flexural strength and fracture toughness of the as-HIPed material are presented in Figs. 4 and 5, respectively. The smooth bars tested under TPB presented linear load–displacement curves up to 900 ºC where brittle to ductile transition takes place. Thus, the bending strength was obtained from the Strength of Materials theory for an elastic beam of square cross-section. As observed in Fig. 4, WCr10Ti2 exhibits a clear increase in strength between 20 and 800 °C, reaching a maximum strength of about 560 MPa and then decreasing in the plastic region. In Fig. 5 the fracture toughness as a function of temperature is plotted. In most cases, the load–displacement curves were linear until fracture and the fracture toughness was computed from the maximum load and the initial notch length in each test using the appropriate expression for the stress intensity factor [11]. The results displayed show that the material appeared to attain the highest values at 900 ºC, i.e. around the DBTT, decreasing beyond this temperature. Its behavior with temperature is consistent with that found for the flexural strength.

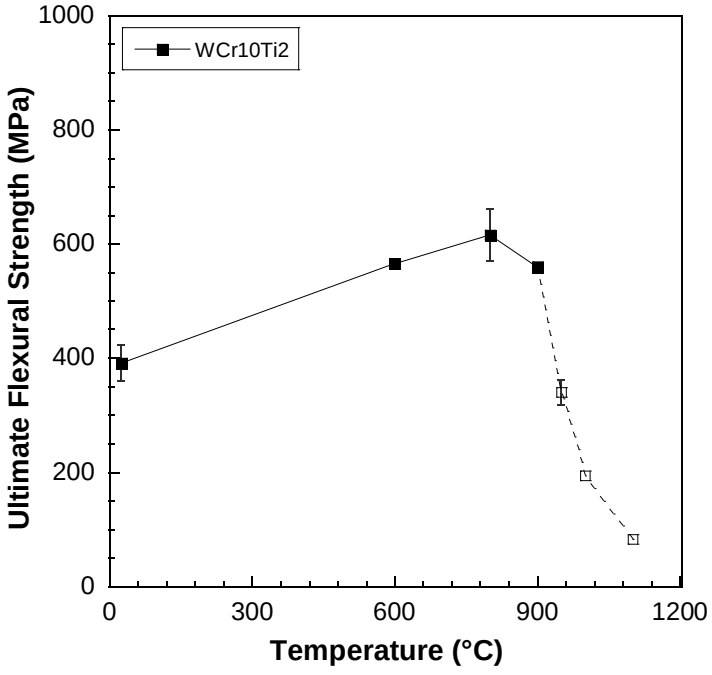

Figure 4. Average flexure strength versus test temperature for WCr10Ti02 after HIP at 1300ºC. Open symbols represent the yield strength at 0.2%.

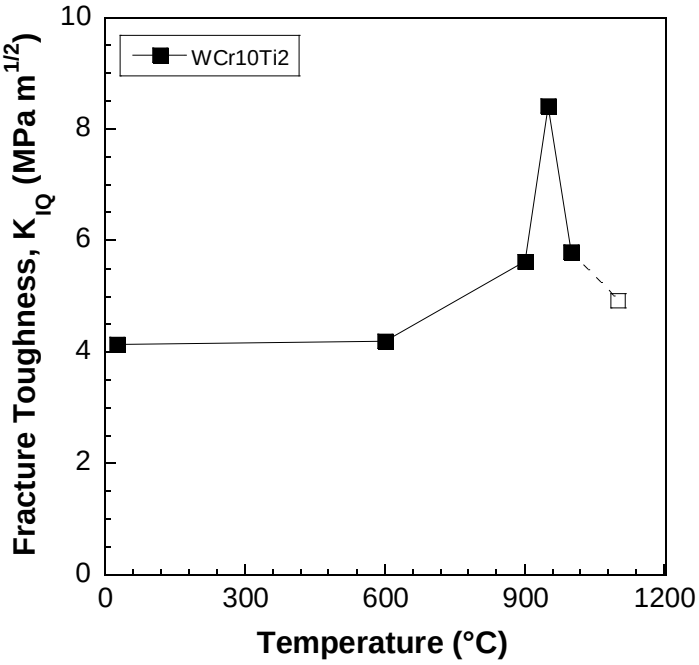

Figure 5. Average fracture toughness versus test temperature for WCr10Ti02 after HIP at 1300ºC. Continuous lines and full symbols represent the linear elastic behavior (fracture toughness) and open symbols denote the plastic behavior (apparent fracture toughness).

3.2. MA + Compaction + Pressureless Sintering in H_2 + HIP without encapsulation

After pressureless sintering at 1600°C the samples of ∅16 mm exhibited 93% relative density whereas those of ∅20 mm did not reach 90% due to the presence of cracks by end-capping. The compaction stage is not easy because of the high hardness and difficult deformation of the alloy powder. For this reason, it was necessary to use a binder. Since the porosity of samples with 93% density was entirely closed, they were HIPped without encapsulation at 1300ºC and 150 MPa for 1 h, achieving 100% density. Nevertheless, the O and C contents of these samples after sintering (Table 1) increased by a factor of about 2 and 4, respectively, compared to the contents after MA due to the binder residue. Again no uptake of contaminants was detected after HIP.

After sintering at 1600°C the microstructure was fine and homogeneous with average grain size about 1 μm (Fig. 1 (c-d)). The main phase corresponds to (αW,Cr) with small amounts of (αCr,W) and Ti-rich phases. The composition of the two bcc phases can be deduced from the shift of the corresponding XRD

peaks (Fig. 2). The (αW,Cr) phase has a Cr content of about 23 at.% while the (αCr,W) phase, with a hardly visible peak, has a W content of about 38 at%. According to the phase diagram, for the present alloy composition at 1600°C only one single bcc phase should be present. The composition of the (αW,Cr) phase corresponds in the W-Cr phase diagram to a temperature of the order of 1450°C. This fact together with the broadness and asymmetric shape of these peaks in the corresponding XRD spectrum of Fig. 2 indicate that longer sintering times would be required to achieve the composition of equilibrium.

After a subsequent HIP cycle at 1300°C the microstructure (Fig. 1 (e-f)) is similar to the one after sintering with the difference of a larger presence of the (αCr,W) phase, as expected. The compositions of the (αW,Cr) and (αCr,W) phases with about 17 at.% Cr and 21 at% W, respectively, correspond to a temperature in the W-Cr phase diagram of about 1350°C, indicating that again longer times are required for achieving the composition of equilibrium.

The Vickers microhardness of the WCr10Ti2 alloy after sintering + HIP (Table 1) is lower than the one of the material produced by the first route due to the grain growth during the sintering at 1600ºC. Using equation (1) to determine the hardness of polycrystalline tungsten with the same grain size, a value of 670 kg/mm^2 is obtained, which is about 20% lower than the microhardness measured for this alloy.

Because of the difficulties in manufacturing large samples no mechanical properties and thermal conductivity have been measured on samples produced by this route.

4. Conclusions

Self-passivating bulk WCr10Ti2 alloys were manufactured by two different powder metallurgical routes. The first route consists of MA followed by HIP of metallic capsules whereas the second one consists of MA, compaction, pressureless sintering in H_2 and subsequent HIPing without encapsulation. Both routes result in fully dense materials with a very fine and homogeneous microstructure consisting of two main phases, (αW,Cr) and (αCr, W), and a minority phase corresponding probably to δ-Ti_2O. Grain sizes about 300 nm and

1 μm were found for the materials produced by the first and the second route, respectively. The content of impurities after MA was reasonably low and remained unchanged after HIP, but it increased after sintering due to the binder residue. It was not possible to produce large samples by the second route due to difficulties in the uniaxial compaction stage. Compaction by cold isostatic pressing in the future would be a feasible way to overcome these problems, avoiding also the use of binder and thus the introduction of undesired contamination.

Flexural strength and fracture toughness was measured on samples produced by the first route. The DBTT is of the order of 900°C. The strength increases from room temperature to 800°C and decreases significantly in the plastic region. An increase of fracture toughness is observed around the DBTT.

Acknowledgments

This work has been carried out within the framework of the EUROfusion Consortium and has received funding from the Euratom research and training programme 2014-2018 under grant agreement No 633053, by the Spanish Ministry of Economy and Competitiveness (ENE2012-30753 and MAT2012-38541-C02-02) and by Comunidad de Madrid (research project S2013/MIT-2862-MULTIMAT-CHALLENGE). The views and opinions expressed herein do not necessarily reflect those of the European Commission.

References

[1] Stork D *et al.* 2014 *Fusion Eng. Des.* **89** 1586

[2] Maisonnier D *et al* 2005 *A Conceptual Study of Commercial Fusion Power Plants*, Final Report, EFDA-RP-RE-5.0

[3] Taylor NP and Pampin R 2006 *Fusion Eng. Des.* **81** 1333

[4] López-Ruiz P, Ordás N, Lindig S, Koch F, Iturriza I and García-Rosales C 2011 *Phys. Scr.* **T145** 014018 (5 pp).

[5] López-Ruiz P, Ordás N, Iturriza I *et al.* 2013 *J. Nucl. Mater.* **442** 219

[6] García-Rosales C, López-Ruiz P, Alvarez-Martín S, Calvo A, Ordás N, Koch F and Brinkmann J 2014 *Fusion Eng. Des.* **89** 1611

[7] Koch F, Köppl S and Bolt H 2009 *J. Nucl. Mater.* **386–388** 572

[8] Koch F, Brinkmann J, Lindig S, Mishra TP and Linsmeier Ch 2011 *Phys. Scr.* **T145** 014019 (5 pp)

[9] Lassner E and Schubert W-D 1998 *Tungsten, properties, chemistry, technology of the element, alloys and chemical compounds* (Vienna University of Technology, Austria)

[10] Palacios T and Pastor JY 2015 Influence of the notch root radius on the fracture toughness of brittle metals: nanostructure tungsten alloy, a case study. Submitted to *Int. J. Refract. Met. Hard Mater.*

[11] Guinea GV, Pastor JY, Planas J and Elices M 1998 *Int. J. Fracture* **89**

[12] Nagender Naidu SV and Rama Rao P 1991 *Phase Diagrams of Binary Tungsten Alloys* (Calcutta, Indian Inst. of Metals)

[13] Vegard L. 1921 *Z. Phys.* **5** 17

[14] Andersson JO, Helander T, Höglund L, Shi PF and Sundman B 2002 *Thermo-Calc and DICTRA, Computational tools for materials science* Calphad, 26, 273-312.

[15] Sikka SK, Vohra YK an Chidambaram R 1982 *Prog. Mater. Sci.* **27** 245

[16] Andersson S 1959 *Acta Chem. Scand.* **13** 415

[17] Akahama Y, Kawamura H and Le Bihan T 2001 *Phys.Rev. Lett.* **87** 275,503

[18] Vegas A *et al*. 2004 *Solid State Sci.* **6** 809